

Unique distant classical Cepheid OGLE GD-CEP-1353 with anomalously high abundances of s- and r-process elements

V. V. Kovtyukh^{1,2}, S. M. Andrievsky^{1,2,3}, K. Werner², and S. A. Korotin⁴

¹ Astronomical Observatory, Odessa National University, Shevchenko Park, 65014, Odessa, Ukraine
e-mail: vkovtyukh@ukr.net

² Institut für Astronomie und Astrophysik, Kepler Center for Astro and Particle Physics, Universität Tübingen, Sand 1, 72076 Tübingen, Germany

³ GEPI, Observatoire de Paris, Université PSL, CNRS, 5 Place Jules Janssen, F-92190 Meudon, France

⁴ Physics of stars department, Crimean Astrophysical Observatory, Nauchny 298409, Republic of Crimea

Received date; accepted: date

ABSTRACT

Aims. While looking for recently discovered distant Cepheids with an interesting chemical composition, we noticed one star (OGLE GD-CEP-1353) with extremely large equivalent widths of spectral lines of heavy elements. The aim of this work is to perform an abundance analysis, and to find a possible explanation for the found chemical anomaly.

Methods. Quantitative analysis of the equivalent widths and synthetic spectrum synthesis were used to derive abundances in this star. Both local and nonlocal thermodynamic equilibrium (LTE and NLTE) approximations were used in our analysis.

Results. Abundances of 28 chemical elements from carbon to thorium were derived. While light and iron peak elements show abundances typical for distant Cepheids (located in the outer disk), the s-process elements are overabundant about one dex. r-process elements are slightly less overabundant. This makes the star a unique Cepheid of our Galaxy.

Key words. Stars: abundances – Stars: variables: Cepheids

1. Introduction

Cepheids are yellow supergiant stars of spectral classes F to K, which are at an evolutionary stage when they are crossing the instability strip in the Hertzsprung-Russell diagram (HRD). During the crossing time, these stars pulsate in radial modes.

Observationally, their atmospheres do not exhibit remarkable chemical peculiarities. A few anomalies that are an inherent feature of Cepheids are connected to their internal structure. After hydrogen depletion in the stellar core, it contracts and heats. A shell source, where fresh hydrogen is converted into helium, develops. At this evolutionary stage, the star expands and settles in the red giant branch (RGB) region. Here the first dredge-up occurs (Iben 1967). To the surface of the star, it brings material processed in the incomplete CNO cycle. Here, carbon is partially converted into nitrogen, and if the first dredge-up happens before nitrogen is converted into oxygen, one can detect that the surface abundances of carbon and nitrogen are altered: carbon is depleted and nitrogen is enhanced (see, for example, the recent large-scale study of the Cepheids' chemical properties by Luck 2018, Fig. 19). This phenomenon is not observed in the F and G unevolved dwarfs (e.g., Reddy et al. 2003). The next stage after the RGB evolution is determined by the helium burning in the stellar core. As the helium in the core ignites in a smooth regime, the star contracts and increases its effective temperature. Thus, the star starts to perform a blue loop in the HRD. At this time interval, the star can be noticed as a Cepheid. This scenario is well known, and its description can be found in many literature sources. What is important is that the Cepheid atmospheres preserve the C–N abundance anomalies. This is a well-established observational fact (see, for example,

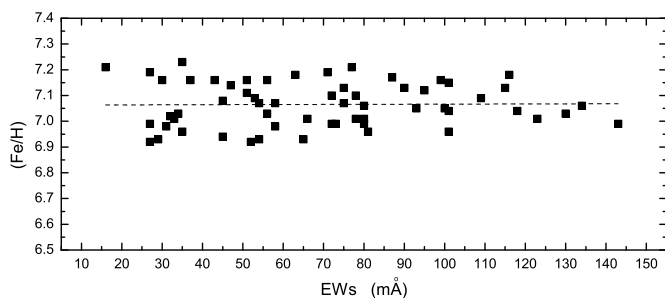
Lambert 1981, Luck & Lambert 1985, Luck 2018 and references therein). Cepheid stars show a slightly increased abundance of sodium (e.g., Andrievsky et al. 2003, Luck 2018). Elements that are formed through the capture of free thermalized neutrons by seed nuclei (s-process elements) normally do not show significantly increased abundances, and this is clear from the evolutionary point of view. The internal structure of Cepheids does not provide a neutron source. Nearly normal relative abundances of the neutron capture elements ($[s/Fe]$) in Cepheids were reported recently by da Silva et al. (2016) and Luck (2018). As a rule, all of the studied heavy element abundances, including r-process elements such as Eu, are in the range from zero to 0.2 dex (s/Fe). For zirconium and lanthanum, abundances are 0.1–0.2 dex higher but, according to Luck (2018), with a big error bar.

In summary, any anomalies of heavy element abundances that can be found in a Cepheid deserve special attention. In this paper we report our detection of remarkable overabundances of s- and r-process elements in the distant classical Cepheid OGLE GD-CEP-1353. Its characteristics are given in Table 1 (together with atmospheric parameters described in the next Section). The high-resolution spectrum of this star was obtained using the Ultraviolet and Visual Echelle Spectrograph (UVES; Dekker et al. 2000) at the Very Large Telescope of ESO at Paranal (Chile). The resolving power and signal-to-noise ratio (S/N) are 42300 and 34, respectively.

Skowron et al. (2019) give the heliocentric (d) and Galactocentric (R_G) distances that we list in Table 1. We note that from the Gaia DR3 (Data Release 3) database OGLE GD-CEP-1353 has a parallax of 0.0815 mas, which means its heliocentric distance is about 12 kpc, being close to above the mentioned value.

Table 1. Some characteristics of our program Cepheid OGLE GD-CEP-1353.

P	JD	phase	$\langle V \rangle$	$\langle I \rangle$	T_{eff}	$\sigma(T_{\text{eff}})$	$\log g$	V_t	l	b	d	R_G
d	2 400 000+		mag	mag	K	K		km s ⁻¹			kpc	kpc
3.1492138	59198.63235	.839	15.501	13.676	5817	± 137	2.00	3.30	247.481	-4.282	11.0	16.0

**Fig. 1.** To the V_t determination (absence of a dependence between the iron abundance of individual lines and their equivalent widths).

The remainder of this paper is organized as follows. In Sect. 2 we describe our abundance analysis of OGLE GD-CEP-1353. In Sect. 3 we discuss our results and present our conclusions.

2. Abundance results

The first attempt to derive abundances in this star was recently made by Trentin et al. (2023) (ASASSN-V J074354.86-323013.7). Their paper lists abundance results for 24 elements from carbon to neodymium for a large number of Cepheids (abundances of only 18 elements were determined for this star; from heavy species only for zirconium and barium). Unfortunately, this unique star was apparently "lost" in the large number of the program stars, and the authors did not pay due attention and did not discuss its individual chemical properties.

2.1. Atmosphere parameters

The effective temperature, T_{eff} , was derived from the line-depth ratios (Kovtyukh 2007), a technique commonly employed in studies of Cepheid variables (e.g., Andrievsky et al. 2016; Luck 2018; Lemasle et al. 2013; da Silva et al. 2022; Kovtyukh et al. 2022). Once T_{eff} is determined, the surface gravity ($\log g$) is found by imposing the iron ionization balance (the same iron abundance derived from the lines of neutral and ionized iron). The microturbulent velocity, V_t , was derived assuming that there is no dependence between the iron abundance, obtained from Fe I lines, and the equivalent widths (EWs) of the same lines (Fig. 1). The adopted value $[\text{Fe}/\text{H}]$ is that, which is derived from the Fe I lines, since we assumed the ionization balance and because they outnumber Fe II lines. The atmospheric parameters T_{eff} , $\log g$, and V_t are listed in Table 1. Since Trentin et al. (2023) used practically the same methods of the atmosphere parameters' determination, we have very close results on the temperature, gravity, and microturbulent velocity.

2.2. LTE results

The abundances of different elements were derived in the LTE approximation using atmosphere models interpolated for the atmosphere parameters within the grid of ATLAS9 models

by Castelli & Kurucz (2004). We discarded strong lines (with $\text{EWs} > 150 \text{ m}\text{\AA}$) due to noticeable damping effects. The list of the lines of the heavy elements measured in the spectrum of our program star is given in Table A.1 of the Appendix. The oscillator strengths, $\log gf$, were adopted from the Vienna Atomic Line Database (VALD, Ryabchikova et al. 2015, version 2023). The reference solar abundances were taken from Asplund et al. (2009) or determined by us in the NLTE calculations.

The abundances of some heavy elements were calculated via direct fitting observed and synthetic profiles of individual spectral lines. We used the SynthV code of Tsymbal et al. (2019) in combination with the ATLAS9 model. LTE approximation was assumed in this spectrum synthesis. Some examples of synthetic spectra fragments are shown in Fig. 2 and 3. All of the results are given in Table 2.

2.3. NLTE results

For some elements we applied the NLTE approximation to derive their abundances. In Table 2 the corresponding ions are marked as NLTE. The atomic models used are described in detail in several papers by the members of our group, for example, carbon (Andrievsky et al. 2001, Lyubimkov et al. 2015), sodium (Korotin & Mishenina 1999, Dobrovolskas et al. 2014), magnesium (Mishenina et al. 2004, Černiauskas et al. 2017), aluminum (Andrievsky et al. 2008, Caffau et al. 2019), sulfur (Korotin 2009, calcium (Andrievsky et al. 2018), and barium (Andrievsky et al. 2009).

The general method of the NLTE calculations we used in our previous papers is the following. In order to find atomic level populations for the ions of interest, we employed the code MULTI (Carlsson 1986). For our aim, this program was modified by Korotin et al. (1999). MULTI allows one to calculate a single NLTE line profile. If the line of interest is blended, we performed the following procedure. With the help of MULTI, we first calculated the departure coefficients for those atomic levels that are responsible for the formation of the considered line. Then we included these coefficients in the LTE synthetic spectrum code SYNTHV (Tsymbal et al. 2019). This allowed us to calculate the source function and opacity for each studied line. Simultaneously, the blending lines were calculated in LTE with the help of the line list and corresponding atomic data from the VALD database (Ryabchikova et al. 2015) in the wavelength range of the line under study. For all our computations, we used 1D LTE atmosphere models computed with the ATLAS9 code by Castelli & Kurucz (2004).

Table 2 shows the averaged individual chemical abundances and their uncertainties. We note that abundance results may suffer from a combined influence of the errors in T_{eff} , $\log g$, V_t , the position of the continuum, and the accuracy of the $\log gf$. Abundances of those elements that are represented in the spectrum by less than three lines must be taken with caution.

The program star abundance pattern that referred to solar abundances is also presented in Fig. 4. The extremely high barium abundance might not be realistic due to the very strong lines of this element. These lines are effectively formed in the upper

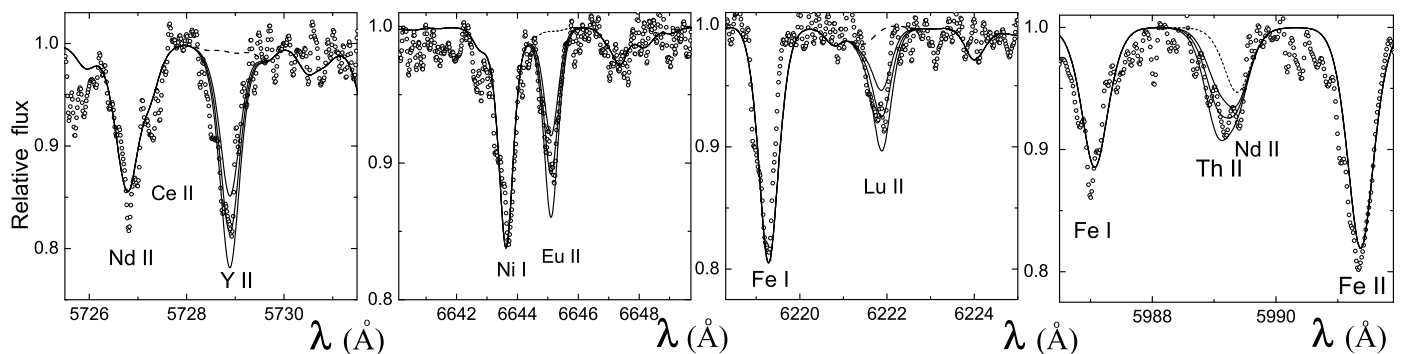


Fig. 2. Observed (open circles) and LTE synthetic profiles of Y II 5728.89 Å, Eu II 6645.10 Å, Lu II 6221.89 Å, and Th II 5989.045 Å lines (solid line). The dashed line indicates no Y, Eu, Lu, or Th. The solid lines show the abundance variation of ± 0.20 dex for these elements and the best fit.

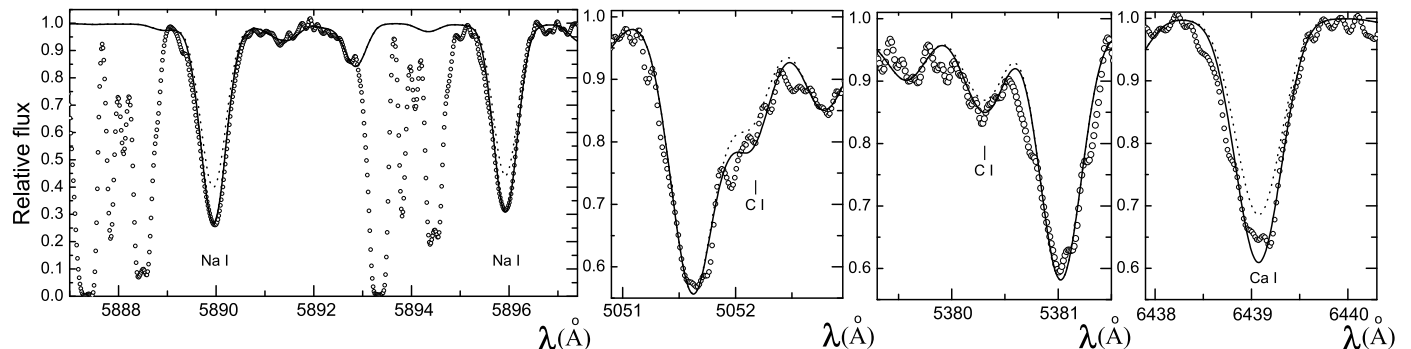


Fig. 3. NLTE profiles of some lines of C, Na, and Ca (solid line) compared to the observed profiles (open circles). LTE profiles were calculated with the same abundances as NLTE profiles (dotted line).

layers of the Cepheid atmosphere, where the microturbulent velocity can significantly exaggerate the value found from the iron lines. We could not account for this possible phenomenon, so we simply state that the barium abundance from our analysis may be overestimated.

As mentioned, all derived abundances were normalized to the iron content in our program star. It should be noted that the iron content in Cepheids shows the expected dependence upon Galactocentric distance: the larger the distance, the lower the iron content. For instance, this is shown in Andrievsky et al. (2016), Luck (2018), Trentin et al. (2023), da Silva et al. (2023), and the references therein. From these data, it can be seen that the distant Cepheids in the outer Galactic disk have an iron content 2–3 times lower than in the Sun (see, for example, Fig. 23 in Luck 2018 based on period–luminosity distances). The distance to our program Cepheid is mentioned in Table 1. Cepheids at such a distance show absolute iron content from 7.0 to 7.4 (7.5 for the Sun), and thus our program star fits in this range.

3. Discussion and conclusion

First of all, it should be noted that none of the Cepheids of our Galaxy studied to date show such an abnormal chemical composition. In some sense, it resembles the chemical composition of the chemically peculiar (CP) stars (Ryabchikova et al. 1997, Yushchenko et al. 2008), or even Przybylski’s star (Shulyak et al. 2010), of course, in a much lesser extent. It is believed that CP stars gain their anomalies from atomic diffusion in the dynamically stable atmospheres (Michaud 1973). This cannot be the case for yellow supergiants with atmospheric convection. As to Przybylski’s star, several hypotheses exist explaining its extreme peculiarities (for more details, readers can refer to

the overview in Andrievsky 2022). In addition, this author considered processes in a binary system consisting of Przybylski’s star and a neutron star, which is the source of high-energy γ radiation, which may affect the atmosphere of Przybylski’s star.

Studying the derived abundance distribution in our program star, we must describe a few characteristic features of it (Fig. 4), namely, the deficiency of iron-peak elements; the rather high relative-to-iron abundance of carbon; the increased sodium abundance, for example for the Cepheids with a pulsational period of 3 days, Genovali et al. 2015 give an average sodium overabundance $[\text{Na}/\text{Fe}]$ of about 0.3 dex, while our program star shows $[\text{Na}/\text{Fe}] = 0.6$ dex; and a significantly increased abundance of the s-process elements (elements that formed as a result of the slow neutron capture by seed nuclei). In addition, the following remarks can be made: there is a fairly high level of overabundance of the light s-process elements (Y, Zr); and with europium, lutetium, and thorium, being r-process elements (rapid neutron capture), they have apparently high abundances, too. We note that according to da Silva et al. (2016) (their Fig. 6), with the relative-to-iron europium abundance $[\text{Eu}/\text{Fe}]$ being extrapolated to a distance of about 12 kpc, it is about zero, while the corresponding value for our program star is 0.6 dex.

As we mentioned in the Introduction, Cepheid atmospheres exhibit the results of the dredge-up event. From the observational point of view, the result of the first dredge-up event was described by Lambert (1981) and Luck & Lambert (1985). After dredge-up carbon becomes deficient, while nitrogen is overabundant. The region of the spectrum of our program star that is available to us does not contain nitrogen lines, so we cannot prove this fact. Yellow supergiant stars and Cepheids, in particular, show a moderate overabundance of sodium (Andrievsky et al. 2003), which can be a sign of the neon-sodium cycle operation. Our

Table 2. LTE and NLTE abundances in OGLE GD-CEP-1353.

Code	Ion	(El/H)	σ	NL	[El/H]	Sun	[El/Fe]	Remark
6.00	C I	8.29	0.06	2	-0.27	8.56	0.24	
6.00	C I	8.00	0.12	3	-0.43	8.43	0.08	NLTE
8.00	O I	8.45	0.15	1	-0.26	8.71	0.25	NLTE
11.00	Na I	6.39	–	1	+0.07	6.32	0.58	
11.00	Na I	6.04	0.12	4	-0.21	6.25	0.30	NLTE
12.00	Mg I	7.48	–	1	-0.20	7.68	0.31	
12.00	Mg I	7.55	0.12	3	+0.01	7.54	0.52	NLTE
13.00	Al I	6.34	0.20	4	-0.09	6.43	0.42	NLTE
14.00	Si I	7.19	0.27	7	-0.41	7.60	0.10	
14.01	Si II	7.39	0.16	2	-0.21	7.60	0.30	
16.00	S I	7.09	–	1	-0.12	7.21	0.39	
16.00	S I	6.64	0.25	5	-0.52	7.16	-0.01	NLTE
20.00	Ca I	6.04	0.16	5	-0.34	6.38	0.17	
20.00	Ca I	5.92	0.10	13	-0.39	6.31	0.12	NLTE
21.01	Sc II	2.89	0.15	4	-0.36	3.25	0.15	
22.00	Ti I	4.69	0.27	3	-0.34	5.03	0.17	
22.01	Ti II	4.53	0.27	3	-0.50	5.03	0.01	
23.00	V I	3.82	–	1	-0.29	4.11	0.22	
24.00	Cr I	5.16	0.14	2	-0.60	5.76	-0.09	
24.01	Cr II	5.26	0.09	3	-0.50	5.76	0.01	
25.00	Mn I	4.95	0.09	3	-0.59	5.54	-0.08	
26.00	Fe I	7.07	0.09	60	-0.51	7.58	0.00	
26.01	Fe II	7.08	0.10	10	-0.50	7.58	0.01	
28.00	Ni I	5.88	0.12	8	-0.42	6.30	0.09	
29.00	Cu I	4.19	0.15	4	-0.06	4.25	0.45	NLTE
39.01	Y II	2.81	0.19	11	+0.62	2.19	1.13	
40.01	Zr II	3.24	0.26	3	+0.36	2.88	0.87	
56.01	Ba II	3.58	0.15	3	+1.41	2.17	1.92	NLTE
57.01	La II	2.18	0.16	16	+0.85	1.33	1.36	
58.01	Ce II	2.46	0.09	18	+0.75	1.71	1.26	
59.01	Pr II	1.26	0.17	6	+0.45	0.81	0.96	
60.01	Nd II	2.18	0.13	35	+0.66	1.52	1.17	
60.02	Nd III	2.12	0.20	1	+0.60	1.52	1.11	
62.01	Sm II	1.82	0.20	6	+0.72	1.10	1.23	
63.01	Eu II	0.76	0.24	1	+0.09	0.52	0.60	synth
68.01	Er II	1.95	0.20	1	+1.03	0.92	1.54	synth
71.01	Lu II	0.60	0.20	1	+0.40	0.10	0.91	synth
90.01	Th II	1.00	0.20	1	+0.98	0.02	1.49	synth

Note 1: NL is the number of lines used.

Note 2: (El/H) is the absolute abundance value on the scale where the hydrogen abundance is 12.00.

NLTE calculations of the sodium abundance in this star confirm this fact. However, increased sodium in our program Cepheid may have another origin.

Nearly normal relative abundances of the neutron capture elements ([s/Fe]) in Cepheids were recently reported by da Silva et al. (2016) and Luck (2018). As it was already mentioned in the Introduction, all studied s-process elements normally do not show significant excesses in the relative-to-iron abundances. If we compare our results on s-process abundances presented in Table 2 with those given in the two abovementioned papers, we would see that Cepheid OGLE GD-CEP-1353 has an overabundance of these elements by several times larger than any studied Cepheid until now (more than 500 stars). It makes this object really unique in our Galaxy. Below we consider several possible hypotheses that may help to understand its unique chemical properties.

Our program star OGLE GD-CEP-1353 has a light curve typical of classical Cepheids (Udalski et al. 2015). Additionally, its Galactic latitude is small (Table 1), which means it can be a

thin disk star. Since its fundamental pulsational period is about 3.15 days, according to Turner (1996) (mass–pulsation period relation), its mass should be about 4 solar masses. The lifetime of a star of this mass (B-star progenitor + following a Cepheid stage), $t \approx 10^{10} (\frac{M_{\odot}}{M_*})^{2.5}$ years, should be about 3.7×10^8 years (the core helium-burning stage takes about 25–30 % of the main-sequence time, see, e.g., Chiosi 1990). According to the age–pulsation period relation by Bono et al. (2005), the age of a Cepheid is 1.1×10^8 years (for [Fe/H]=−0.5).

1. Suppose now that this Cepheid had a companion of a slightly higher mass. After a certain time, such a companion ends its evolution as an asymptotic giant branch (AGB) star. Having finished this evolutionary stage, the envelope of this rather massive AGB star (more than 4 solar masses) could contaminate the present Cepheid’s atmosphere (or its B-star progenitor), enriching it in s-process elements. The more massive component after all becomes a C–O white dwarf. This scenario can explain the appearance of the s-process elements in the Cepheid’s atmosphere. More massive AGB stars produce a larger amount of

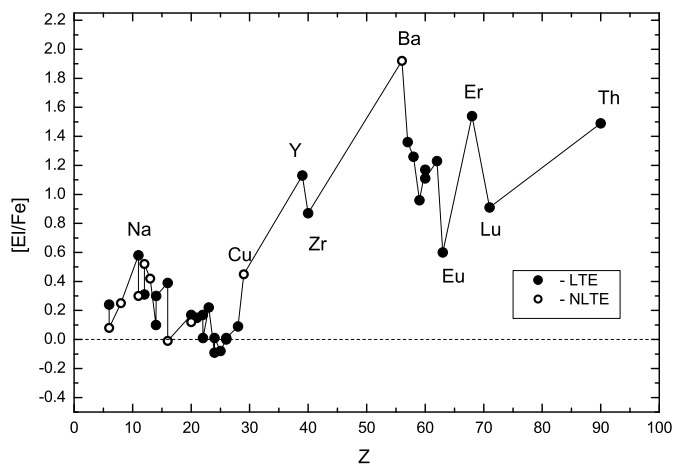


Fig. 4. Graphical representation of the content of Table 2.

the weak s-process elements, such as yttrium and zirconium, and this is seen in our program Cepheid (see, Fig. 4).

According to Goswami & Goswami (2023), see their Fig. 14 Panel a, the AGB model of 4 solar masses with a metallicity of about -0.5 (recall that the iron peak elements in our program star show the same abundance level) yield enough the s-process elements, and the light s-process elements (Sr, Y, and Zr) are at the same abundance level as the heavy s-process elements (Ba–Sm), $[E/Fe] \approx 0.8 - 0.9$. This is exactly what we see in our program Cepheid. It should be noted that in the lower-mass AGB stars, the light s-process elements are less abundant compared to the heavy s-process elements. Finally, as is mentioned above, sodium is apparently increased in our program star. This may be connected to the fact that the highest sodium production is reached in 4 solar mass AGB stars (Di Criscienzo et al. 2016).

However, despite its attractiveness, this hypothesis faces a problem with unexpectedly high abundances of the typical r-process elements, such as europium, lutetium, and thorium. As believed, the nuclei of these heavy elements cannot be formed inside the AGB star because of the insufficient neutron flux. The typical neutron density in the low-mass AGB stars is about 10^7 cm^{-3} (Straniero et al. 2006).

2. This Cepheid has a companion of a significantly higher mass. In this case its companion ended its evolution as a neutron star after the Supernova II (SN II) explosion. For this to happen, the B-star progenitor must have a mass larger than 8 solar masses. If it was a close explosion, the possibility of a single contamination event would be possible. However, there is one weak place in this hypothesis. Even for the lower limit of the SN II mass, the expected lifetime of its progenitor B star is about 6×10^7 years. Soon after this time, the star explodes. Its companion (presently a Cepheid) is still evolving as a late B star. If the atmosphere of this B star is contaminated, then after the following evolution to the red giant stage and first dredge-up, all of the material synthesized in the SN explosion that contaminated the B star atmosphere will be mixed with the stellar interior. Thus, the surface abundance anomalies will hardly survive.

3. Finally, suppose that the OGLE GD-CEP-1353's more massive companion ended its evolution as a neutron star. If this neutron star is a source of γ radiation and if this radiation is directed toward the present-day Cepheid atmosphere, then one can expect that irradiation of the atmosphere gas will produce free neutrons. Such free neutrons (provided their flux is sufficiently high) can lead to the production of the s- and r-process elements. A similar mechanism was proposed by Andrievsky (2022) to ex-

plain the phenomenon of a chemically peculiar Przybylski's star (see details in that paper).

An additional question may arise concerning the first and third scenario. How long can the contaminated atmosphere of the Cepheid star preserve the chemical composition abundance anomalies? To estimate the characteristic time, we used the following formula (Sweet 1950): $t = 8 \times 10^{12} \frac{M^3}{LR^4 \Omega^2}$ years.

All values here are in solar units. As previously mentioned, the mass of our program star with its pulsation period of about 3 days, is about 4 solar masses. According to Gieren et al. (1999), a Cepheid with such a period has a radius of about 30 solar radii. The period – luminosity relation gives the luminosity of this star of about $10^3 L_{\odot}$. To determine the angular rotation velocity of the Cepheid (the radii of the Cepheid and the Sun are known), we adopted a typical radius of its progenitor, the main-sequence B star, to be about $3.3 R_{\odot}$, and a linear equatorial velocity about 200 km s^{-1} (a very rough estimate according to Brott et al. 2011 gives $v \sin i$ of about 100 km s^{-1} for stars of about 10 solar masses, see their Fig. 1). Then, after expanding from 3 to $30 R_{\odot}$, the rotational velocity of the Cepheid decreased to a few km s^{-1} (approximately the same as the solar rotational rate). All adopted values give us a characteristic time of the large-scale meridional circulation of about 5×10^8 years or more. This value exceeds our program Cepheid lifetime (see the estimate above).

To evaluate the validity of the hypothesis described above, a necessary condition has to be met. One needs to prove that OGLE GD-CEP-1353 is a component of a binary system with a secondary component being a compact object. Regarding the OGLE GD-CEP-1353 visual magnitude, it seems to be impossible now.

In summary, we have described a very unusual chemical composition of this star, in particular the high abundance of heavy elements in its atmosphere. It may be a component of a binary system originally consisting of two stars with slightly or moderately different masses. The further evolution of the stars in this system led to contamination of the OGLE GD-CEP-1353 atmosphere with heavy elements, and thus forming in this way its unique chemical properties.

Acknowledgements. Based on observations made with ESO Telescopes at the Paranal Observatories under programme ID 0106.D-0561(A). VVK and SMA are grateful to DAAD (German Academic Exchange Service) for financial support. SMA would also like to thank ESO at Garching for support during his stay in Germany, which enabled him to perform part of this work. We are grateful to our referee for his/her very detailed review and helpful comments.

References

- Andrievsky S.M., 2022, *Odessa Astron. Publ.*, 35, 13
 Andrievsky S. M., Kovtyukh V. V., Korotin S. A., Spite M., Spite F., 2001, *A&A*, 367, 605
 Andrievsky S.M., Egorova I.A., Korotin S.A., Kovtyukh V.V., 2003, *Astron. Nachr./AN324*, No. 6, 532
 Andrievsky S. M., Spite M., Korotin S. A., Spite F., Bonifacio P., Cayrel R., Hill V., Francois P., 2008, *A&A*, 481, 481
 Andrievsky S.M., Spite M., Korotin S.A., et al., 2009, *A&A*, 494, 1083
 Andrievsky S.M., Martin R.P., Kovtyukh V.V., Korotin S.A., Lépine J.R.D., 2016, *MNRAS*, 461, 4256
 Andrievsky S.M., Bonifacio P., Caffau E., Korotin S.A., Spite M., Spite F., Sbordone L., Zhukova A.V., 2018, *MNRAS*.473.3377
 Asplund M., Grevesse N., Sauval A. J., Scott P., 2009, *ARA&A*, 47, 481
 Bono G., Marconi M., Cassisi S., Caputo F., Gieren W., Pietrzynski G., 2005, *ApJ*, 621, 966
 Brott I., de Mink S.E., Cantiello M., Langer N., de Koter A., Evans C.J., Hunter I., Trundle C., Vink J.S., 2011, *A&A*530, A115
 Caffau E. et al., 2019, *A&A*, 628, A46
 Carlsson M., 1986, *Uppsala Astron. Obs. Publ.*, 33
 Castellì F., Kurucz R.L., 2004, arXiv:astro-ph/0405087

- Černiauskas A. et al., 2017, A&A, 604, A35
- Chiosi C., 1990, PASP, 102, 412
- da Silva R., Lemasle B., Bono G., et al., 2016, A&A, 586A.125
- da Silva R., Crestani J., Bono G. et al., 2022, A&A, 661A.104D
- da Silva R., d’Orazi V., Palla M., Fabrizio M. et al., 2023, arXiv:2308.01928
- Dekker H., D’Odorico S., Kaufer A., Delabre B., & Kotzlowski H., 2000, in Proc. SPIE, Vol. 4008, Optical and IR Telescope Instrumentation and Detectors, ed. M. Iye & A. F. Moorwood, 534-545
- Di Criscienzo M., Ventura P., García-Hernández D.A., Dell’Agli F., Castellani M., Marrese P.M., Marinoni S., Guiffrida S., Zamora O., 2016, MNRAS, 462, 395
- Dobrovolskas V., Kučinskas A., Bonifacio P. et al., 2014, A&A, 565, A121
- Genovali K., Lemasle B., da Silva R., Bono G., Fabrizio M. et al., 2015, A&A, 580, id.A17
- Gieren W.P., Moffet T.J., Barnes III T.G., 1999, ApJ 512, 553
- Goswami P.P, Goswami A., 2023, ApJ, 165, 154
- Iben I., 1967, ARA&A, 5, 5711
- Kervella P., Gallenne A., Evans N.R., Szabados L., Arenou F., Mérand A., Nardetto N., Gieren W., Pietrzynski G., 2019, A&A, 623, A117
- Korotin S. A., 2009, Astron. Rep., 53, 651
- Korotin S. A., Andrievsky S. M., Luck R. E., 1999, A&A, 351, 168
- Korotin S.A., Mishenina T.V., 1999, Astron. Rep., 43, 533
- Kovtyukh V.V., 2007, MNRAS, 378, 617
- Kovtyukh V. Lemasle B., Bono G., Usenko I.A., da Silva R., Kniazev A., Grebel E.K., Andronov I.L., Shakun L., Chinarova L., 2022, MNRAS, 510, 1894
- Lambert D.L., 1981, In: Physical processes in red giants; Proceedings of the Second Workshop, Erice, Italy, September 3-13, 1980. (A82-33776 16-90) Dordrecht, D. Reidel Publishing Co., 1981, p. 115–134
- Lemasle B., François P., Genovali K., et al., 2013, A&A, 558, 31
- Luck R.E., 2018, ApJ, 156, 171
- Luck R.E., Lambert D.L., 1985, ApJ, 298, 782
- Lyubimkov L.S., Lambert D.L., Korotin S.A., Rachkovskaya T.M., Poklad D.B., 2015, MNRAS, 446, 3447
- Michaud G., 1973, Astrophys. Lett., 15, 143
- Mishenina T. V., Soubiran C., Kovtyukh V. V., Korotin S. A., 2004, A&A, 418, 551
- Reddy B.E., Tomkin J., Lambert D.L., Allende Prieto C., 2003, MNRAS, 340, 304
- Ryabchikova T.A., Adelman S.J., Weiss W.W., Kuschnig R., 1997, A&A, 322, 234
- Ryabchikova T., Piskunov N., Kurucz R. L., Stempels H. C., Heiter U., Pakhomov Y., Barklem P. S., 2015, Physica Scripta, 90, 054005
- Shulyak D., Ryabchikova T., Kildiyarova R., Kochukhov O., 2010, A&A, 520, A88
- Skowron D.M., Skowron J., Mróz P., Udalski A., Pietrukowicz P., Soszyński I., Szymański M.K., Poleski R., Kozłowski S., Ulaczyk K., Rybicki K., Iwanek P., Wrona M., Gromadzki M., 2019, Aca, 69, 305
- Spite, M., Andrievsky, S. M., Spite, F., et al. 2012, A&A, 541, A143
- Straniero O., Gallino R., Cristallo S., 2006, NuPhA, 777, 311
- Sweet P.A., 1950, MNRAS, 110, 548
- Trentin E., Ripepi V., Catanzaro G., Storm J., Marconi M., De Somma G., Testa V., Musella I., 2023, MNRAS, 519, 2331
- Tsymbal V., Ryabchikova T., Sitnova T., 2019, in Kudryavtsev D. O., Romanyuk I. I., Yakunin I. A., eds, Astronomical Society of the Pacific Conference Series, Vol. 518, Physics of Magnetic Stars. pp 247-252
- Turner D., 1996, JARSC, 90, 82
- Udalski A., Szymański M.K., Szymański G., 2015, Acta Astron., 65, 1
- Yushchenko V., Gopka V., Yushchenko A., Shavrina A., Hubrig S., Musaev F., 2008, Odessa Astron. Publ., 21, 153

Appendix A:

Table A.1. Equivalent widths (in mÅ) of the lines used for the calculation of the abundances of elements (for LTE calculations we used lines with EW<150 mÅ only).

Wavelength (Å)	Ion	EW (mÅ)	log gf	E _{low} (eV)	(E _I /H)
5380.3370	6.00	69.8	-1.615	7.685	8.33
6587.6100	6.00	47.4	-1.021	8.537	8.25
6160.7470	11.00	72.7	-1.245	2.104	6.39
5711.0880	12.00	124.6	-1.723	4.346	7.48
5948.5410	14.00	79.8	-1.130	5.082	7.10
6125.0210	14.00	38.8	-1.464	5.614	7.43
6155.1340	14.00	62.8	-0.754	5.619	7.03
6237.3190	14.00	48.5	-0.974	5.614	7.05
6244.4650	14.00	31.8	-1.090	5.616	6.94
6414.9800	14.00	29.1	-1.035	5.871	7.07
6721.8480	14.00	38.1	-1.526	5.863	7.70
6347.1090	14.01	109.1	0.170	8.121	7.28
6371.3710	14.01	110.3	-0.039	8.121	7.50
6748.7900	16.00	36.0	-0.529	7.868	7.09
5349.4650	20.00	123.6	-0.309	2.709	6.10
5581.9650	20.00	122.1	-0.554	2.523	6.13
5590.1140	20.00	88.5	-0.571	2.521	5.75
5601.2770	20.00	125.6	-0.522	2.526	6.14
6166.4390	20.00	66.6	-1.142	2.521	6.06
5318.3490	21.01	53.7	-2.014	1.357	3.01
5667.1490	21.01	111.8	-1.309	1.500	3.02
6245.6370	21.01	113.6	-1.021	1.507	2.72
6604.6010	21.01	110.8	-1.308	1.357	2.80
5210.3850	22.00	125.5	-0.849	0.048	4.76
6258.7060	22.00	74.1	-0.239	1.460	4.92
6261.0970	22.00	21.5	-0.478	1.430	4.40
5211.5300	22.01	103.2	-1.159	2.590	4.29
5268.6150	22.01	105.0	-1.669	2.598	4.82
6606.9500	22.01	31.5	-2.789	2.061	4.49
6090.2140	23.00	31.5	-0.061	1.081	3.82
5329.1380	24.00	52.6	-0.007	2.914	5.06
5348.3150	24.00	127.6	-1.210	1.004	5.26
5334.8690	24.01	73.6	-1.825	4.072	5.18
5420.9220	24.01	59.6	-2.457	3.758	5.35
5502.0670	24.01	47.4	-2.116	4.168	5.24
6013.5100	25.00	59.0	-0.351	3.072	5.00
6016.6700	25.00	73.8	-0.182	3.073	5.00
6021.8200	25.00	70.8	-0.053	3.075	4.84
4950.1060	26.00	57.7	-1.669	3.417	6.98
5029.6180	26.00	34.1	-2.049	3.415	7.03
5049.8200	26.00	190.4	-1.354	2.279	7.21
5090.7740	26.00	108.8	-0.399	4.256	7.09
5198.7110	26.00	123.3	-2.134	2.223	7.01
5217.3890	26.00	134.1	-1.074	3.211	7.06
5242.4910	26.00	115.1	-0.967	3.634	7.13
5243.7770	26.00	51.2	-1.149	4.256	7.16
5339.9290	26.00	170.5	-0.646	3.266	7.16
5373.7090	26.00	52.5	-0.859	4.473	7.09
5383.3690	26.00	192.4	0.645	4.313	7.17
5389.4790	26.00	100.9	-0.409	4.415	7.15
5391.4590	26.00	66.4	-0.920	4.154	7.01
5398.2790	26.00	71.9	-0.669	4.446	7.10
5466.3960	26.00	71.8	-0.629	4.371	6.99
5554.8950	26.00	79.8	-0.439	4.549	7.06
5560.2120	26.00	27.0	-1.189	4.435	6.99
5565.7040	26.00	93.4	-0.212	4.608	7.05
5638.2620	26.00	89.8	-0.720	4.220	7.13
5679.0230	26.00	46.7	-0.820	4.652	7.14

Table A.1. continued.

Wavelength (Å)	Ion	EW (mÅ)	log gf	Elow (eV)	(El/H)
5686.5300	26.00	74.9	-0.570	4.549	7.13
5731.7620	26.00	34.5	-1.200	4.256	6.96
5752.0320	26.00	27.2	-1.010	4.549	6.92
5753.1230	26.00	78.1	-0.687	4.260	7.01
5859.5860	26.00	77.0	-0.630	4.549	7.21
5862.3560	26.00	98.9	-0.330	4.549	7.16
5883.8170	26.00	55.6	-1.260	3.960	7.03
5984.8150	26.00	80.3	-0.195	4.733	6.99
5987.0650	26.00	54.2	-0.520	4.796	7.07
6003.0120	26.00	72.7	-1.100	3.882	6.99
6008.5560	26.00	94.8	-0.985	3.884	7.12
6027.0510	26.00	52.1	-1.089	4.076	6.92
6056.0050	26.00	64.7	-0.320	4.733	6.93
6065.4820	26.00	158.8	-1.529	2.609	7.16
6151.6180	26.00	32.8	-3.295	2.176	7.01
6165.3600	26.00	37.4	-1.473	4.143	7.16
6173.3360	26.00	54.4	-2.880	2.223	6.93
6213.4300	26.00	101.0	-2.481	2.223	7.04
6215.1440	26.00	50.9	-1.190	4.186	7.11
6219.2810	26.00	101.3	-2.432	2.198	6.96
6229.2280	26.00	32.3	-2.670	2.845	7.02
6232.6410	26.00	86.9	-1.360	3.654	7.17
6240.6460	26.00	29.4	-3.230	2.223	6.93
6246.3190	26.00	130.4	-0.771	3.603	7.03
6252.5550	26.00	167.3	-1.699	2.404	7.21
6265.1340	26.00	100.4	-2.550	2.176	7.05
6270.2250	26.00	55.9	-2.470	2.858	7.16
6322.6860	26.00	74.9	-2.430	2.588	7.07
6336.8240	26.00	118.4	-0.852	3.686	7.04
6355.0290	26.00	70.9	-2.349	2.845	7.19
6358.6980	26.00	57.7	-4.340	0.859	7.07
6380.7430	26.00	30.5	-1.375	4.186	6.98
6408.0180	26.00	116.0	-1.017	3.686	7.18
6419.9500	26.00	80.1	-0.239	4.733	7.01
6430.8460	26.00	159.6	-2.005	2.176	7.17
6475.6240	26.00	42.6	-2.941	2.559	7.16
6481.8700	26.00	63.4	-2.981	2.279	7.18
6494.9810	26.00	207.8	-1.268	2.404	7.26
6498.9390	26.00	35.0	-4.698	0.958	7.23
6518.3670	26.00	45.3	-2.560	2.832	7.08
6592.9140	26.00	143.4	-1.472	2.728	6.99
6593.8710	26.00	81.3	-2.421	2.433	6.96
6597.5610	26.00	27.1	-1.069	4.796	7.19
6609.1100	26.00	45.0	-2.691	2.559	6.94
6627.5450	26.00	16.2	-1.590	4.549	7.21
6733.1510	26.00	29.5	-1.150	4.638	7.16
6750.1530	26.00	77.8	-2.618	2.424	7.10
4993.3580	26.01	123.3	-3.639	2.807	7.13
5100.6640	26.01	59.7	-4.169	2.807	6.94
5256.9370	26.01	67.2	-4.181	2.891	7.11
5414.0730	26.01	98.7	-3.539	3.221	7.12
5627.4970	26.01	39.6	-4.129	3.387	7.18
5991.3760	26.01	115.6	-3.539	3.153	7.22
6084.1110	26.01	64.2	-3.779	3.199	6.94
6113.3220	26.01	50.7	-4.109	3.221	7.13
6369.4620	26.01	68.0	-4.159	2.891	7.05
6416.9190	26.01	109.2	-2.649	3.892	6.97
6446.4100	26.01	40.7	-1.959	6.223	7.68
5694.9830	28.00	32.1	-0.609	4.089	5.83
5754.6560	28.00	50.3	-2.329	1.935	5.73

Table A.1. continued.

Wavelength (Å)	Ion	EW (mÅ)	log gf	Elow (eV)	(El/H)
6086.2810	28.00	35.3	-0.529	4.266	5.96
6108.1160	28.00	58.2	-2.600	1.676	5.83
6111.0700	28.00	28.3	-0.869	4.088	6.01
6186.7110	28.00	25.4	-0.959	4.105	6.06
6767.7720	28.00	84.8	-2.140	1.826	5.77
6772.3150	28.00	35.3	-0.979	3.658	5.81
4883.6821	39.01	303.2	0.070	1.084	3.36
5087.4190	39.01	248.1	-0.170	1.084	3.11
5119.1120	39.01	148.3	-1.359	0.992	2.92
5200.4097	39.01	243.2	-0.570	0.992	3.33
5289.8166	39.01	64.6	-1.850	1.032	2.50
5320.7831	39.01	34.9	-1.950	1.084	2.27
5402.7742	39.01	162.0	-0.630	1.839	3.18
5473.3853	39.01	131.3	-1.020	1.738	3.07
5480.7303	39.01	148.7	-0.990	1.721	3.23
5509.8948	39.01	204.8	-1.010	0.992	3.22
5521.5500	39.01	98.6	-0.635	1.738	2.63
5544.6114	39.01	110.9	-1.090	1.738	2.91
5546.0088	39.01	127.0	-1.100	1.748	3.11
5662.9241	39.01	217.8	0.200	1.944	3.12
5728.8865	39.01	81.6	-1.120	1.839	2.72
6613.7317	39.01	111.2	-1.110	1.748	2.87
6795.4156	39.01	109.9	-0.913	1.738	2.75
5350.3500	40.01	91.3	-1.160	1.773	3.32
6100.1210	40.01	70.9	-1.500	1.756	3.37
6114.8520	40.01	51.0	-1.400	1.665	2.94
5853.6680	56.01	369.2	-0.999	0.604	3.88
6141.7130	56.01	543.3	-0.075	0.704	3.62
6496.8970	56.01	502.0	-0.376	0.604	3.68
4804.0400	57.01	110.8	-1.490	0.235	2.16
4809.0000	57.01	119.1	-1.400	0.235	2.17
5156.7300	57.01	86.9	-1.850	0.126	2.12
5303.5300	57.01	124.5	-1.350	0.321	2.20
5377.0520	57.01	42.4	-0.430	2.304	2.34
5381.9100	57.01	30.6	-0.720	2.134	2.28
5482.2700	57.01	54.5	-2.230	0.000	2.00
5671.5280	57.01	21.4	-0.870	2.210	2.31
5863.6900	57.01	77.5	-1.370	0.927	2.29
5936.2100	57.01	56.6	-2.060	0.173	2.00
6126.0750	57.01	52.0	-1.240	1.252	2.19
6129.5560	57.01	87.9	-1.500	0.772	2.36
6172.7210	57.01	53.7	-2.320	0.126	2.16
6320.3760	57.01	131.3	-1.610	0.173	2.28
6390.4800	57.01	138.2	-1.410	0.321	2.30
6671.4040	57.01	51.4	-2.030	0.403	2.09
5037.7996	58.01	82.0	-0.570	1.008	2.48
5117.1690	58.01	76.9	-0.049	1.402	2.30
5117.9455	58.01	37.2	-0.810	1.247	2.43
5386.7730	58.01	48.5	-0.710	1.212	2.43
5435.2435	58.01	42.6	-2.000	0.000	2.42
5468.3710	58.01	78.2	-0.070	1.402	2.30
5472.2791	58.01	112.8	-0.100	1.247	2.54
5516.0816	58.01	31.6	-0.570	1.615	2.43
5518.4889	58.01	57.8	-0.650	1.155	2.41
5561.4450	58.01	26.5	-0.880	1.458	2.49
5613.6940	58.01	44.7	-0.640	1.420	2.50
5623.0011	58.01	39.9	-1.150	0.956	2.48
5695.8474	58.01	35.1	-0.610	1.626	2.53
5933.5816	58.01	43.4	-1.770	0.327	2.50
5941.5447	58.01	49.5	-0.940	1.107	2.53

Table A.1. continued.

Wavelength (Å)	Ion	EW (mÅ)	log gf	Elow (eV)	(El/H)
5959.6878	58.01	31.7	-0.690	1.626	2.54
6043.3730	58.01	84.9	-0.480	1.206	2.55
6051.8154	58.01	63.5	-1.530	0.232	2.39
6272.0254	58.01	54.7	-0.400	1.544	2.47
6652.7390	58.01	33.5	-0.580	1.528	2.33
5034.4060	59.01	28.7	-0.090	1.111	1.12
5135.1400	59.01	45.7	0.008	0.950	1.12
5219.0450	59.01	58.9	-0.052	0.795	1.18
5220.1079	59.01	92.5	0.298	0.796	1.18
5322.7710	59.01	83.6	-0.318	0.483	1.38
6017.7990	59.01	31.0	-0.257	1.112	1.27
6025.7170	59.01	35.2	0.067	1.440	1.34
4917.3800	60.01	60.9	-1.440	0.559	2.43
4943.8990	60.01	76.2	-1.640	0.205	2.44
4947.0200	60.01	50.8	-1.130	0.559	2.00
4949.0110	60.01	33.6	-1.450	0.630	2.15
4998.5410	60.01	83.4	-1.100	0.471	2.23
5063.7200	60.01	65.1	-0.620	0.976	2.06
5089.8320	60.01	78.8	-1.160	0.205	1.97
5092.7900	60.01	146.6	-0.610	0.380	2.36
5181.1690	60.01	74.8	-0.599	0.859	2.02
5182.5900	60.01	78.7	-0.910	0.745	2.25
5212.3600	60.01	132.6	-0.960	0.205	2.33
5255.5056	60.01	161.6	-0.670	0.205	2.40
5272.0460	60.01	42.0	-1.070	0.986	2.23
5276.8690	60.01	82.8	-0.440	0.859	1.93
5306.4600	60.01	42.6	-0.970	0.859	2.01
5310.0400	60.01	23.4	-0.980	1.137	1.97
5311.4500	60.01	115.6	-0.420	0.986	2.39
5356.9700	60.01	95.6	-0.280	1.264	2.31
5361.4670	60.01	155.0	-0.370	0.680	2.49
5385.8880	60.01	77.5	-0.819	0.742	2.13
5385.8880	60.01	87.7	-0.820	0.742	2.24
5416.3740	60.01	62.8	-0.930	0.859	2.20
5421.5510	60.01	76.7	-1.330	0.380	2.26
5431.5200	60.01	86.5	-0.469	1.121	2.25
5442.2640	60.01	69.1	-0.910	0.680	2.07
5447.5550	60.01	57.1	-1.050	1.044	2.44
5449.2200	60.01	50.4	-0.690	1.264	2.22
5485.7000	60.01	104.3	-0.120	1.264	2.23
5508.3980	60.01	60.8	-1.230	0.859	2.47
5533.8200	60.01	70.2	-1.230	0.559	2.27
5548.4500	60.01	68.4	-1.270	0.550	2.28
5550.0800	60.01	46.3	-0.980	1.228	2.42
5595.8020	60.01	31.5	-1.530	0.859	2.38
5603.6500	60.01	33.5	-1.690	0.380	2.09
5620.5943	60.01	71.5	-0.310	1.545	2.35
5625.7300	60.01	36.2	-1.120	0.933	2.12
5659.7750	60.01	27.1	-0.520	1.600	2.03
5702.2400	60.01	90.1	-0.880	0.745	2.30
5726.8300	60.01	78.9	-0.810	1.044	2.42
5740.8600	60.01	72.6	-0.530	1.160	2.19
5742.0900	60.01	42.6	-0.830	1.091	2.07
5743.1925	60.01	36.5	-0.730	1.282	2.07
5744.7770	60.01	43.9	-1.030	0.986	2.18
5865.0270	60.01	29.1	-0.830	1.410	2.17
6031.2700	60.01	37.0	-0.740	1.282	2.07
6183.9000	60.01	45.4	-0.920	1.160	2.24
6330.1510	60.01	27.5	-0.720	1.773	2.37
6382.0600	60.01	43.2	-0.750	1.436	2.31

Table A.1. continued.

Wavelength (Å)	Ion	EW (mÅ)	log gf	Elow (eV)	(El/H)
6385.1870	60.01	72.0	-0.360	1.600	2.41
6637.9600	60.01	45.0	-0.320	1.773	2.22
6650.5200	60.01	40.4	-0.110	1.953	2.13
6737.7600	60.01	39.5	-0.670	1.600	2.32
5294.1133	60.02	78.8	-0.690	0.000	2.12
4815.8000	62.01	127.1	-0.820	0.185	1.94
4844.2088	62.01	94.0	-0.890	0.278	1.73
4948.6300	62.01	39.3	-0.950	0.544	1.42
4961.9400	62.01	74.6	-1.090	0.434	1.87
5052.7500	62.01	55.0	-0.160	1.375	1.66
6731.8100	62.01	30.3	-0.739	1.166	1.58
6645.0940	63.01	60.9	0.120	1.380	0.77
6221.8900	71.01	55.4	-0.760	1.542	0.83
5989.0450	90.01	50.2	-1.414	0.189	1.12